mathematics

MDPI

Article

Simultaneous Features of CC Heat Flux on Dusty Ternary Nanofluid (Graphene + Tungsten Oxide + Zirconium Oxide) through a Magnetic Field with Slippery Condition

Basma Souayeh [1,2]

[1] Department of Physics, College of Science, King Faisal University, P.O. Box 400, Al-Ahsa 31982, Saudi Arabia; bsouayeh@kfu.edu.sa or basma.souayeh@gmail.com

[2] Laboratory of Fluid Mechanics, Physics Department, Faculty of Sciences of Tunis, University of Tunis El Manar, Tunis 2092, Tunisia

Abstract: The purpose of this work is to offer a unique theoretical ternary nanofluid (graphene/tungsten oxide/zirconium oxide) framework for better heat transfer. This model describes how to create better heat conduction than a hybrid nanofluid. Three different nanostructures with different chemical and physical bonds are suspended in water to create the ternary nanofluid (graphene/tungsten oxide/zirconium oxide). Toxic substances are broken down, the air is purified, and other devices are cooled thanks to the synergy of these nanoparticles. The properties of ternary nanofluids are discussed in this article, including their thermal conductivity, specific heat capacitance, viscosity, and density. In addition, heat transport phenomena are explained by the Cattaneo–Christov (CC) heat flow theory. In the modeling of the physical phenomena under investigation, the impacts of thermal nonlinear radiation and velocity slip are considered. By using the right transformations, flow-generating PDEs are converted into nonlinear ordinary differential equations. The parameters' impacts on the velocity and temperature fields are analyzed in detail. The modeled problem is graphically handled in MATLAB using a numerical technique (BVP4c). Graphical representations of the important factors affecting temperature and velocity fields are illustrated through graphs. The findings disclose that the performance of ternary nanofluid phase heat transfer is improved compared to dusty phase performance. Furthermore, the magnetic parameter and the velocity slip parameter both experience a slowing-down effect of their respective velocities.

Keywords: slip flow; CC heat flux; suspended particles; ternary nanoparticles; nonlinear radiation

MSC: 76-10

Citation: Souayeh, B. Simultaneous Features of CC Heat Flux on Dusty Ternary Nanofluid (Graphene + Tungsten Oxide + Zirconium Oxide) through a Magnetic Field with Slippery Condition. *Mathematics* **2023**, *11*, 554. https://doi.org/10.3390/math11030554

Academic Editors: Mohsen Sharifpur, Josua P. Meyer and S. Suseel Jai Krishnan

Received: 20 December 2022
Revised: 15 January 2023
Accepted: 18 January 2023
Published: 20 January 2023

1. Introduction

Nanofluids are liquids that include ultrafine particles contained in a dilute solution. These particles are suspended in the liquid. These fluids have thermophysical qualities that are far better than those of pure fluids. It has been established that increasing the amount of carbon, copper, or other nanoparticles with high thermal conductivity that is added to water, ethylene glycol, or oil may enhance the materials' ability to transport heat. The thermal conductivity of the nanofluids is significantly raised, and the particle size and volume fraction of suspended particles have an impact on this phenomenon. Choi [1] invented the term "nanofluids", which defines a liquid suspension of ultrasmall particles (less than 50 nm in diameter). With the fast development of nanofabrication, various affordable combinations of fluid/particles are instantly accessible. A complete assessment by Buongiorno [2] investigated convective transport in nanofluids, who argued that an appropriate explanation for the phenomenon exists, although unexpected growth in heat conductivity and viscosity is yet to be found. Recently, Reddy et al. [3] investigated hybrid dusty fluid flow through a Cattaneo–Christov heat flux model. Waqas et al. [4] discussed the

heat transfer analysis of hybrid nanofluid flow with thermal radiation through a stretching sheet. Gurdal et al. [5] studied the turbulent flow and heat transfer characteristics of Ferro-nanofluid flowing in a dimpled tube under a magnetic field effect. Many researchers [6–9] have addressed the convective heat transfer during the flow of nanoliquid.

The passage of heat energy through the particles of a liquid may be described as a sort of heat transfer known as thermal radiation. It is a condition that must be met in a wide variety of applications, such as the planning of propulsion devices for space spacecraft, nuclear power plants, and gas turbines. In space applications, where devices are required to operate at high temperatures to obtain the required thermal efficiency, the impact of thermal radiation on controlling the heat transfer in certain applications and on estimating the thermal effects for processes with high temperatures is unavoidable. This is because thermal radiation has an impact on both controlling the heat transfer in certain applications and on estimating the thermal effects for processes with high temperatures. Duwairi and Duwairi [10] studied gray viscous fluid flow with magnetic and radiation parameters influences. Cortell [11] analyzed radiation and viscous dissipation impacts for the flow of the thermal boundary layer along a nonlinear stretching surface. Recently, Bakar and Soid [12] studied the MHD stagnation-point flow and heat transfer over an exponentially stretching/shrinking vertical sheet in a micropolar fluid with a buoyancy effect. Ali et al. [13] analyzed the flow and heat transfer over stretching/shrinking and porous surfaces. Azam et al. [14] discussed the transient bioconvection and activation energy impacts on Casson nanofluid with gyrotactic microorganisms and nonlinear radiation. Reddy et al. [15] studied the unsteady absorption flow and dissipation heat transfer over a non-Newtonian fluid. Gnaneswara et al. [16] investigated the effect of thermal conductivity on Blasius–Rayleigh–Stokes flow and heat transfer over a moving plate by considering the magnetic dipole moment. Some recent studies related to the consideration of heat transfer theory can be found in [17–22].

Fourier's law of heat conduction describes heat transfer in a given medium due to temperature differences [23]. It is considered the basis for the investigation of thermal phenomena. Using this law, the temperature field equation is developed into a parabolic-type equation stating that heat transfer with initial disruption having infinite speed propagates throughout the medium under certain conditions. This heat conduction paradox requires modification of Fourier's law. Cattaneo [24] presented a modified form of Fourier's law known as the Maxwell–Cattaneo (MC) model by introducing the thermal relaxation time parameter. This modification converted the temperature field equation from a parabolic- to a hyperbolic-type equation, describing that heat transfer has finite speed in the entire medium. Christov [25] investigated the frame invariance of the MC model and replaced the time derivative with Oldroyd's upper-convected time derivative. Recently, Reddy et al. [26] studied zero-mass flux and Cattaneo–Christov heat flux through a Prandtl non-Newtonian nanofluid in Darcy–Forchheimer porous space. Machireddy et al. [27] investigated the impact of Cattaneo–Christov heat flux on the hydromagnetic flow of non-Newtonian fluids filled with a Darcy–Forchheimer porous medium. Khan et al. [28] discussed Cattaneo–Christov (CC) heat and mass fluxes in the stagnation-point flow of Jeffrey nanoliquids by a stretching surface. Tausif et al. [29] investigated the modified homogeneous and heterogeneous chemical reaction and flow performance of Maxwell nanofluid with the Cattaneo–Christov heat flux law. Some recent studies related to the consideration of CC theory can be found in [30–32].

In this study, we investigated dusty fluid flow subjected to a magnetic field over a stretching sheet. Impacts of thermal radiation, velocity slip, and conditions are considered in the modeling of the physical phenomena. The use of CC heat flux theory is carried out in the energy equation for analyzing the heat transfer phenomena. Considering the appropriate variables, the governing PDEs are converted to nonlinear ODEs. MATLAB software is used for investigating the numerical solution. Impacts of fluid velocity and temperature are analyzed through different pertinent parameters in the considered problem.

Specifically, this work will address the research questions mentioned below:

- What will be the influence of the magnetic parameter on fluid heat transfer rate, temperature, and velocity?
- What is the significance of the CC theory on the dusty ternary fluid model?
- What will be the impact of thermal radiation on heat transfer rate and temperature?
- What will be the influence of the velocity slip parameter on fluid velocity, temperature, and heat transfer rate?

We organized this article as follows. In Section 2, we formulate the physical phenomena of the problem and transformations of PDEs. Result analyses are provided in Section 3. Concluding remarks of the present article are given in Section 4.

2. Mathematical Formulation

Consider a continuous 2D boundary layer flow and the heat transfer of a dusty ternary nanofluid across a stretching sheet moving at a constant speed $U_w = bx$. With the slot serving as the point of origin, the x-axis is drawn along the surface that is being stretched in the direction that the motion is going, and the y-axis is drawn perpendicular to the sheet in the direction that is facing away from the fluid. It is presumable that the flow will not extend beyond the area where y is greater than 0. Convective heat transfer is responsible for keeping the temperature of the sheet's surface at a constant value known as T_f.

Some of the assumptions taken into consideration are listed below:

- The dust particles are taken to be small enough and of sufficient number to be treated as a continuum and allow concepts such as density and velocity to have physical meaning.
- The dust particles are assumed to be spherical in shape, having the same radius and mass, and are undeformable.
- The Cartesian coordinate system is located in such a way that the x-axis and y-axis are taken along (and normal to) the surface, respectively, while the origin of the system is located at the leading edge.
- The dust particles are assumed to be uniform in size, and the density number of the dust particle is taken as constant throughout the flow.

The equations that regulate the flow of dusty ternary nanofluid can be written as follows, according to the standard boundary layer approximations (Reddy et al. [3]):

$$\frac{\partial u}{\partial x} + \frac{\partial v}{\partial y} = 0 \tag{1}$$

$$u\frac{\partial u}{\partial x} + v\frac{\partial u}{\partial y} = \frac{\mu_{thnf}}{\rho_{thnf}}\frac{\partial^2 u}{\partial y^2} - \frac{\sigma B_0^2}{\rho_{thnf}}u \tag{2}$$

$$\left(\rho c_p\right)_{thnf}\left(u\frac{\partial T}{\partial x} + v\frac{\partial T}{\partial y}\right) + \lambda_1\left(\begin{array}{c} u^2\frac{\partial^2 T}{\partial x^2} + v^2\frac{\partial^2 T}{\partial y^2} + 2uv\frac{\partial^2 T}{\partial x \partial y} + \\ \left(u\frac{\partial u}{\partial x} + v\frac{\partial u}{\partial y}\right)\frac{\partial T}{\partial x} + \left(u\frac{\partial v}{\partial x} + v\frac{\partial v}{\partial y}\right)\frac{\partial T}{\partial y} \end{array}\right) = k_{thnf}\frac{\partial^2 T}{\partial y^2} + \frac{Nc_{pf}}{\tau_t}\left(T_p - T\right) + \frac{N}{\tau_v}\left(u_p - u\right)^2 + \frac{1}{\rho c_p}\frac{\partial q_r}{\partial y} + \mu_{thnf}\left(\frac{\partial u}{\partial y}\right)^2 \tag{3}$$

Dust Phase

$$\frac{\partial u_p}{\partial x} + \frac{\partial v_p}{\partial y} = 0 \tag{4}$$

$$u_p\frac{\partial u_p}{\partial x} + v_p\frac{\partial u_p}{\partial y} = \frac{K}{m}(u - u_p) \tag{5}$$

$$\left(u_p\frac{\partial T_p}{\partial x} + v_p\frac{\partial T_p}{\partial y}\right) = \frac{c_{thpf}}{c_{thmf}\tau_T}(T - T_P) \tag{6}$$

By using the Rosseland approximation to the radiative heat flow expression found in Equation (3), one obtains the following:

$$q_r = -\frac{4\sigma^*}{3k^*}\frac{\partial T^4}{\partial y} = -\frac{16\sigma^*}{3k^*}T^3\frac{\partial T}{\partial y} \tag{7}$$

where x and y, respectively, represent coordinate axes along the continuous surface in the direction of motion and perpendicular to it. $(u,\ v)$ and $(u_p,\ v_p)$ denote the velocity components of the nanofluid and dust phases along the x- and y-directions, respectively. N is the number density of dust particles. λ_1 is the thermal relaxation time. m is the mass concentration of dust particles. $K = 6\pi\mu_{nf}\ r$ is the Stokes drag constant. r is the radius of dust particles. A is the slip constant. σ^* is the Stefan–Boltzmann constant. k^* is the mean absorption coefficient.

Boundary Conditions:

$$\begin{aligned} u = U_w + A\nu_f\frac{\partial u}{\partial y},\quad v = 0,\quad -k_f\frac{\partial T}{\partial y} = h_f\Big(T_f - T\Big) \quad \text{at } y = 0,\\ u \to 0,\quad u_p \to 0,\quad v_p \to v,\quad T \to T_\infty,\quad T_p \to T_\infty \quad as \quad y \to \infty, \end{aligned} \tag{8}$$

The expression for viscosity (μ_{thnf}), density (ρ_{thnf}), specific heat ($(\rho Cp)_{thnf}$), and thermal conductivity (k_{thnf}) of the ternary nanofluid is as follows (Prakash et al. [9]):

$$\mu_{thnf} = \frac{\mu_f}{(1-\phi_1\ )^{2.5}(1-\phi_2\ )^{2.5}(1-\phi_3\ )^{2.5}},\ (\rho Cp)_{thnf} = \begin{bmatrix} (1-\phi_2)[(1-\phi_1)(\rho Cp)_f \\ +\phi_1(\rho Cp)_{s1}] + \phi_2(\rho Cp)_{s2} \end{bmatrix},$$

$$\rho_{thnf} = (1-\phi_1)\left[(1-\phi_2)\left\{\begin{matrix}(1-\phi_3)\rho_f\\ +\phi_3\rho_3\end{matrix}\right\} + \phi_2\rho_2\right] + \phi_1\rho_1,$$

$$\frac{k_{thnf}}{k_{hnf}} = \frac{k_1+2k_{hnf}-2\phi_1\left(k_{hnf}-k_1\right)}{k_1+2k_{hnf}+\phi_1\left(k_{hnf}-k_1\right)},\ \frac{k_{hnf}}{k_{nf}} = \frac{k_2+2k_{nf}-2\phi_2\left(k_{nf}-k_2\right)}{k_2+2k_{nf}+\phi_2\left(k_{hnf}-k_2\right)},\ \frac{k_{nf}}{k_{nf}} = \frac{k_3+2k_f-2\phi_3\left(k_f-k_3\right)}{k_3+2k_{nf}+\phi_3\left(k_f-k_3\right)}$$

where ϕ_1, ϕ_2, and ϕ_3 are the nanoparticle volume fraction of copper/alumina/zirconium oxide, respectively. C_p is the specific heat. k_f denotes the thermal conductivity of the regular fluid.

The nonlinear PDEs in the model problem are converted to nonlinear ODEs by way of a similarity transformation, as shown below.

$$\begin{aligned} u = bxf'(\eta), v = -\sqrt{b\nu_f}f(\eta), u_p = bxF'(\eta), v_p = -\sqrt{b\nu_f}F(\eta)\eta = \sqrt{\frac{b}{\nu_f}}y, \theta(\eta) = \frac{T-T_\infty}{T_f-T_\infty},\\ \theta_p(\eta) = \frac{T_p-T_\infty}{T_f-T_\infty} \end{aligned} \tag{9}$$

with $T = T_f(1+(\theta_w-1)\theta)$ and $\theta_w = \frac{T_f}{T_\infty}$, $\theta_w > 1$ the temperature ratio parameter.

Equations (1) and (4) are completely satisfied by these transformations, and the other equations in the model, [2,3,5,6], together with the boundary conditions, are translated as follows:

Fluid Phase:

$$\frac{\mu_{thnf}}{\rho_{thnf}}f''' + \Big(ff'' - f'^2\Big) + \mu_{thnf}\left[l\beta_v\left(F'-f'\right) - QF'\right] = 0. \tag{10}$$

$$\frac{k_{thnf}}{k_f}\left(\theta'' + R\left[(1+(\theta_w-1)\theta)^3\theta'' + 3(\theta_w-1)\theta'^2(1+(\theta_w-1)\theta)^2\right]\right) + \Pr\frac{(\rho cp)_f}{(\rho cp)_{thnf}}\begin{bmatrix}\Gamma\left(ff'\theta' - f^2\theta'\right)\\ +f\theta' + l\beta_T\left[\theta_p-\theta\right]\\ +lEc\beta_v[F'-f']^2\end{bmatrix} + PrEcf''^2 = 0. \tag{11}$$

Dust Phase

$$FF'' - F'^2 + \beta_v\left(f'-F'\right) = 0 \tag{12}$$

$$\theta_p'F + \alpha\beta_T\left(\theta_p-\theta\right) = 0 \tag{13}$$

$$f(0)=0,\ \ f'(0) = 1 + \frac{\delta}{(1+\phi_1)^{2.5}(1+\phi_2)^{2.5}(1+\phi_2)^{2.5}}f''(0),\ \ \theta'(0) = -B_i(1-\theta(0)),$$
$$f'(\infty)\to 0,\ \ F'(\infty)\to 0,\ \ F(\infty)\to f(\infty),\ \ \theta(\infty)\to 0,\ \ \theta_p(\infty)\to 0. \tag{14}$$

where $Q = \frac{\sigma B_0^2}{\rho_f}, \Pr = \frac{\left(\mu c_p\right)_f}{k_f}, Ec = \frac{U_w^2}{\left(T_f-T_\infty\right)c_{pf}}, R = \frac{4\sigma^* T_\infty^3}{3k_{thnf}k^*}$, $\beta_T = \frac{1}{\tau_T c}$, $\beta_v = \frac{1}{\tau_v c}$, $\tau_v = \frac{m}{K}$, $l = \frac{mN}{\rho_f}, \gamma = \frac{c_{pf}}{c_{mf}}$ $\Gamma = b\lambda_1, \delta = A\frac{U_w}{\nu_f}$ and $Bi = \sqrt{\frac{\nu_f}{c}}\frac{h_f}{k_f}$.

The physical quantities of C_f and Nu are;

$$C_f = \frac{\tau_w}{\rho_f U_w^2}, Nu = \frac{xq_w}{k_f\left(T_f - T_\infty\right)} \text{ at } y = 0,$$

where τ_w and q_w are given by

$$\tau_w = \mu_{thnf}\left(\frac{\partial u}{\partial y}\right) q_w = -k_{thnf}\left(\frac{\partial T}{\partial y}\right) \text{ at } y = 0.$$

In terms of the nondimensional variables, we express them as

$$C_f Re^{-\left(\frac{1}{2}\right)} = \left(\frac{\mu_{thnf}}{\mu_f}\right) f''(0) \text{ and } \ Nu(Re)^{-\left(\frac{1}{2}\right)} = -\frac{k_{thnf}}{k_f}\left[1 + R\theta_w^3\right]\theta'(0).$$

where Re $= \frac{U_w^2}{b\upsilon_f}$ is the local Reynolds number.

3. Numerical Method

Solving the nonlinear system of ODEs generated by a numerical technique (BVP4c) in MATLAB (see Equations (10)–(13)) may be achieved numerically with the aid of boundary constraints using the approach described in Equation (14). Table 1 shows the physical properties of the ternary nanofluid. Equations of a higher level of order differential type are produced. A variety of physical influences on the velocity and temperature profiles for both dusty and ternary nanofluid cases are analyzed graphically. Calculated values for $C_f(Re)^{\frac{1}{2}}$, and $Nu(Re)^{-\frac{1}{2}}$ are tabulated below (Tables 3 and 4). At the outset, we reduce these ODEs to the first-order form by simplifying the higher-order terms.

Let $f = y_1$, $f' = y_2$, $f'' = y_3$, $f''' = y_4$, $\theta = y_5$, $\theta' = y_6$, $\theta'' = y_7$ $F = y_8$, $F' = y_9$, $F'' = y_{10}$, $\theta_p = y_{11}$, $\theta_p' = y_{12}$.

Fluid Phase:

$$y_4 = -\frac{\rho_{thnf}}{\mu_{thnf}}\left[\left(y_1y_3 - y_2^2\right) + \mu_{thnf}[l\beta_v(y_9-y_2) - Qy_2]\right], \tag{15}$$

$$y_7 = -\frac{k_f}{k_{thnf}}\left[\begin{array}{c}\left(1+R\left[\begin{array}{c}(1+(\theta_w-1)y_5)^3+\\ 3(\theta_w-1)y_6^2(1+(\theta_w-1)y_5)^2\end{array}\right]\right)+\\ \Pr\frac{(\rho cp)_f}{(\rho cp)_{thnf}}\left[\begin{array}{c}\Gamma\left(y_1y_2y_6-y_1^2y_6\right)\\ +y_1y_6+l\beta_T[y_{11}-y_5]\\ +lEc\beta[y_9-y_2]^2\end{array}\right]+PrEcy_3^2.\end{array}\right], \tag{16}$$

Dust Phase:

$$y_{10} = \frac{1}{y_8}\left[y_9^2-\beta_v(y_2-y_9)\right] \tag{17}$$

$$y_{12} = \frac{1}{y_8}[-\alpha\beta_T(y_{11}-y_5)] \tag{18}$$

Boundary Conditions:

$$\begin{array}{c}(0)=0,\ y_2(0)=1+\frac{\delta}{(1+\varnothing)^{2.5}}y_3(0),\ y_6(0)=-B_i(1-y_5(0)),\ y_2(\infty)\to 0,\ y_9(\infty)\to 0,\\ y_8(\infty)\to y_1(\infty),\ y_5(\infty)\to 0,\ y_{11}(\infty)\to 0\end{array} \tag{19}$$

Table 1. Thermophysical properties of a ternary nanofluid (graphene + sirconium oxide + tungsten oxide) (Prakasha et al. [9]) and Muhammad et al. [33]).

Thermophysical Properties	Base Fluid	Ternary Nanofluid		
	H_2O	Graphene	Zirconium Oxide	Tungsten OXIDE
$\rho(\mathrm{kg/m^2})$	997.1	2200	5680	7160
C_p (j/kgK)	4179	5000	502	96.15
k(w/mk)	0.613	790	1.7	1.63

4. Results and Discussion

In this paper, our study is focused on the dusty ternary nanofluid flow with the Cattaneo–Christov model over a stretching sheet in the presence of a magnetic field, nonlinear radiation, and convective heat transfer. We analyzed the effects of the physical parameters on the velocity and thermal fields through figures and tables by using the fixed parametric values $\Pr = 6.9$, $Ec = 0.5$, $R = 0.6$, $\theta_w = 1.2$, $\delta = 0.7$, $Q = 0.5$, $Bi = 0.8$, $\phi_1 = \phi_2 = \phi_3 = 0.005$, and $\Gamma = 0.4$. Additionally, the results of the comparison of the Prandtl number to previously published studies are shown in Table 2. We can conclude that the current results are in excellent agreement with previous findings in the literature. Furthermore, $C_f(Re)^{\frac{1}{2}}$ and $Nu(Re)^{-\frac{1}{2}}$ values for the present analysis are computed and given in Tables 3 and 4.

Table 2. Validation of the results in comparison with those found in the literature.

Pr	Ghadikolaei et al. [34]	Hosseinzadeh et al. [35]	Reddy et al. [3]	Present Results
0.7	0.4538	0.4541	0.4539	0.45415
2.0	0.9113	0.9114	0.9113	0.91133
7.0	1.8954	1.8954	1.8954	1.89545

Table 3. The friction factor values for various pertinent parameters.

Q	δ	ϕ_1	ϕ_2	ϕ_3	Friction Factor	
					Dusty Phase	Ternary Phase
0.5					0.785239	1.511657
1.0					0.613042	1.447579
1.5					0.508094	1.406297
	0.5				0.620207	1.470950
	1.0				0.541187	1.464362
	1.5				0.446056	1.453310
		0.005			0.740501	1.477960
		0.001			0.688252	1.475486
		0.015			0.640870	1.472762
			0.005		0.967495	1.480191
			0.001		0.828302	1.475561
			0.015		0.549498	1.460959
				0.005	0.740501	1.477961
				0.001	0.688252	1.475486
				0.015	0.549498	1.460959

Table 4. The Nusselt number values for various pertinent parameters.

Pr	Ec	Bi	Γ	R	θ_w	ϕ_1	ϕ_2	ϕ_3	Nusselt Number	
									Dust Phase	Ternary Phase
0.5									1.44697	1.56233
1.0									1.46193	2.69770
1.5									1.48274	3.51973
	0.1								1.50243	1.94796
	0.3								1.43731	1.93508
	0.5								1.39414	1.92532
		0.1							1.51166	2.23259
		0.2							1.44758	1.74300
		0.3							1.40634	1.44461
			0.1						1.57142	1.97687
			0.2						1.84996	2.01510
			0.3						2.08391	2.01747
				0.5					1.45866	1.91198
				1.0					1.53613	1.88219
				1.5					1.57934	1.86686
					0.8				1.28682	1.48919
					1.2				1.32862	1.64629
					1.4				1.36865	1.79380

Table 4. *Cont.*

Pr	*Ec*	*Bi*	Γ	*R*	θ_w	ϕ_1	ϕ_2	ϕ_3	Nusselt Number	
									Dust Phase	Ternary Phase
						0.005			1.06239	1.88550
						0.001			1.16455	1.89615
						0.015			1.27872	1.91104
							0.005		1.39414	1.92532
							0.001		1.43731	1.93508
							0.015		1.51166	2.23259
								0.005	1.17455	1.87615
								0.001	1.22872	1.89104
								0.015	1.30414	1.92532

Figure 1 shows how Q affects the velocity field ($f'(\eta)$ and $F'(\eta)$) for both ternary nanofluid and dusty fluid cases. A decreasing trend can be observed in $f'(\eta)$ and $F'(\eta)$ scenarios for boosting values of Q. Physically, the magnetic field depends on Lorentz force, which is stronger for a larger magnetic field. Therefore, the velocity profile declines with more magnetic fields. In addition, the influence of the ternary nanofluid is examined more thoroughly than in the case of dusty fluid. In addition, the appropriate layer thickness is scaled back in both scenarios when the Q value is increased.

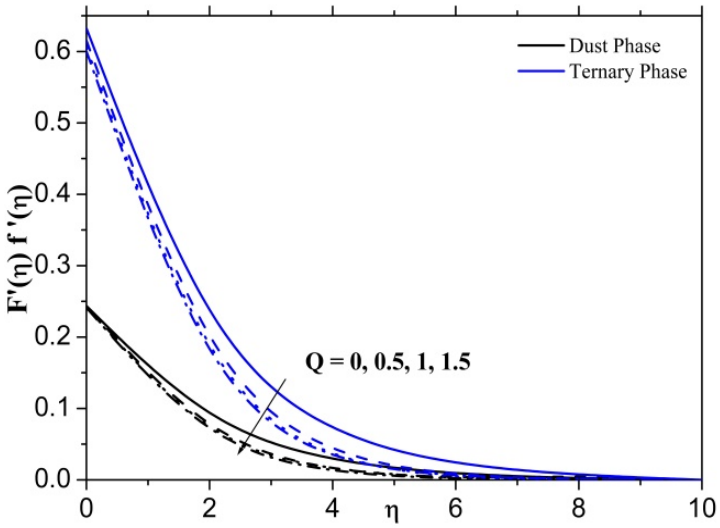

Figure 1. The $f'(\eta)$ and $F'(\eta)$ illustration against Q.

Figures 2–4 depict the instances of dusty fluid and ternary nanofluid and the influence of ϕ_1, ϕ_2, and ϕ_3 on the $F'(\eta)$ and $f'(\eta)$ profiles, respectively. A decrease in the velocity curve that occurs as a consequence of the incorporation of solid nanoparticles (ϕ_1, ϕ_2, and ϕ_3) into the nanomaterial was seen in both dusty and ternary nanofluid cases. This outcome is due to collisions between nanoparticles that have been extensively dispersed across the environment.

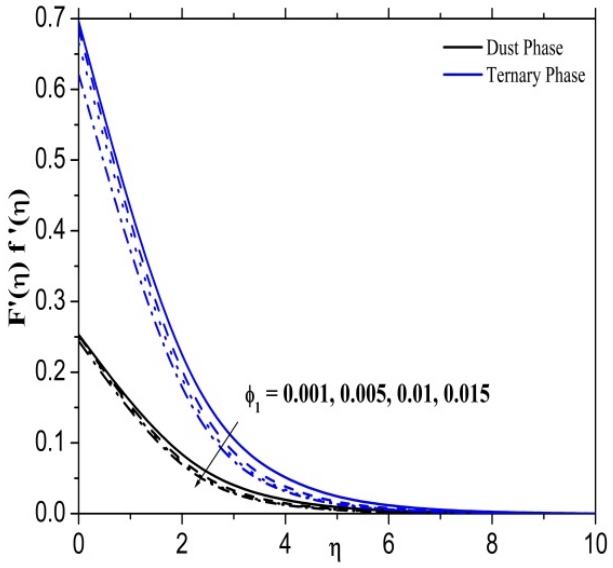

Figure 2. The $f'(\eta)$ and $F'(\eta)$ illustration against ϕ_1.

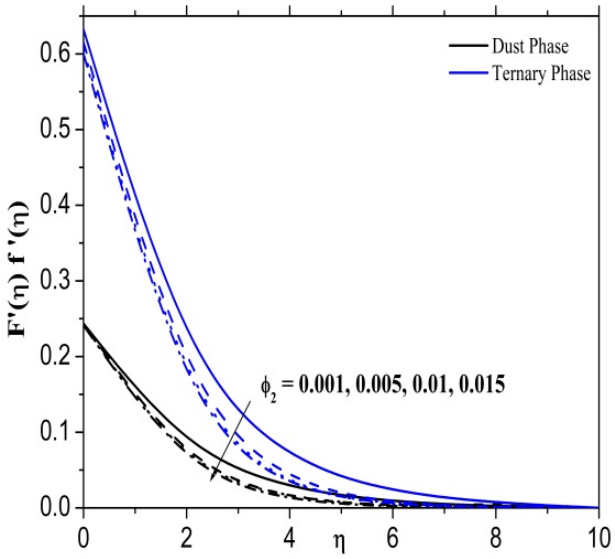

Figure 3. The $f'(\eta)$ and $F'(\eta)$ illustration against ϕ_2.

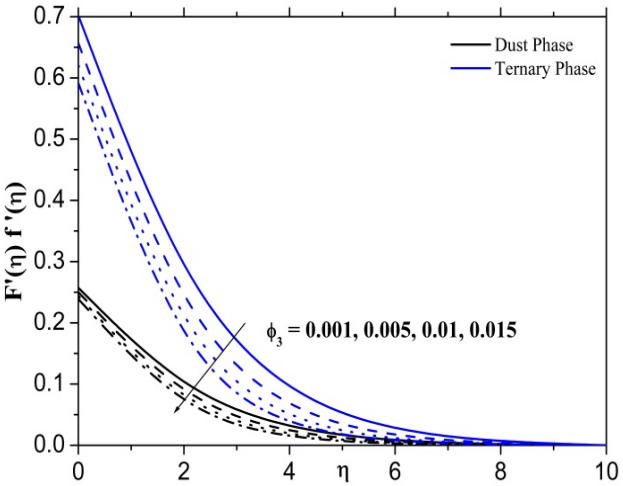

Figure 4. The $f'(\eta)$ and $F'(\eta)$ illustration against ϕ_3.

In order to explore the impact of the δ parameter on the velocity distributions of the $F'(\eta)$ and $f'(\eta)$ profiles, Figure 5 is displayed. It is clear from these results that changing the value of the parameter results has a significant reduction of the velocity distribution for both the $F'(\eta)$ and $f'(\eta)$ situations. This is due to the fact that the fluid's near-surface velocity does not sustain correctly for the extended surface velocity when taking slip effect into consideration. Therefore, if the value of the slip velocity parameter is increased, the slide speed will be increased accordingly. Following this, there is a decrease in the liquid velocity as a result of the stretching surface deformation, which can only be communicated to the fluid under slip conditions.

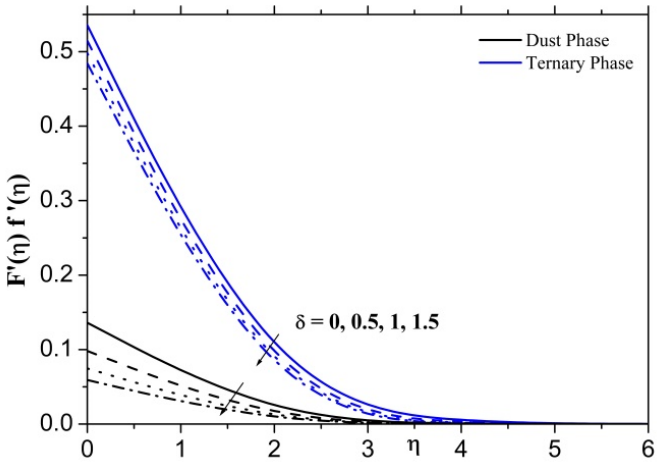

Figure 5. The $f'(\eta)$ and $F'(\eta)$ illustration against δ.

In Figure 6, we can see how R affects the temperature field for both ternary nanofluid phase and dusty phase ($\theta(\eta)$ and $\theta_p(\eta)$) profiles. It seems to be enhanced when R improves. In accordance with the physical principle, as the radiation parameter increases, heat is radiated at the fluid at a much higher rate than when the mean absorption coefficient decreases. Physically, the effect of thermal radiation is to boost the transfer, as by increasing thermal radiation, the thermal boundary layer increases. Therefore, it has been reported that the process of thermal radiation reduction should proceed at a faster rate. The use of radiation can regulate the distribution of temperature and flow, and such applications can be used in pseudoscience to monitor blood pressure via the magnetotherapy process.

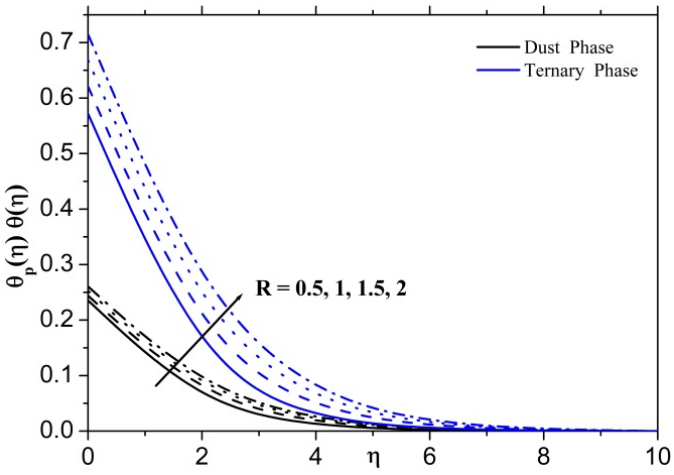

Figure 6. The $\theta(\eta)$ and $\theta_p(\eta)$ illustration against R.

Figure 7 depicts the analysis of the characteristics of the function $\theta(\eta)$ and $\theta_p(\eta)$ in relation to rising values of θ_w for a ternary nanofluid and dusty fluid condition, respectively.

It is witnessed that the thermal field and thermal layer thickness of the ternary nanofluid and dusty fluid condition both increase at an exponential rate when the θ_w parameter is increased. In addition, for high values of θ_w, a rise in fluid temperature enriches the whole fluid case. This is the situation when the temperature of the fluid is increased. In addition, the enhancement of fluid temperature is optimal in the case of the ternary nanofluid, followed by the case of dusty fluid.

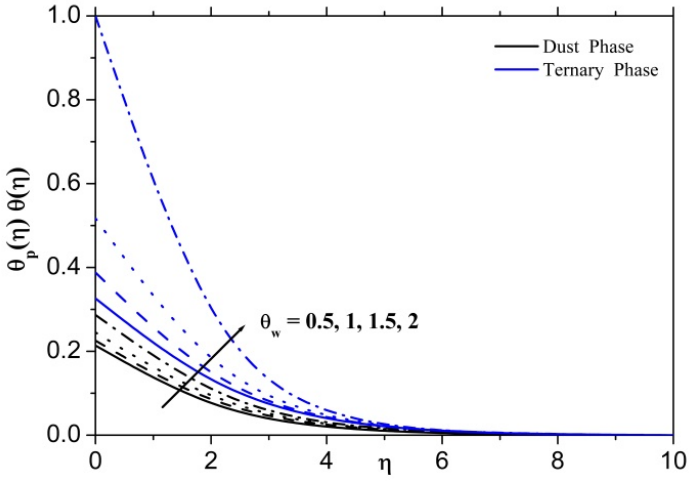

Figure 7. The $\theta(\eta)$ and $\theta_p(\eta)$ illustration against θ_w.

Figure 8 displays the changes in the thermal field for the ternary nanofluid and dusty fluid instances as a function of the *Ec* parameter. To improve the *Ec* parameter, it is evident that the thermal field rises in both ternary nanofluid and dusty fluid phases. Physically, the Eckert number is the ratio of kinetic energy to the specific enthalpy difference between wall and fluid. Therefore, an increase in the Eckert number causes the transformation of kinetic energy into internal energy by work that is done against the viscous fluid stresses. Due to this, increasing *Ec* enhances dramatically the temperature of the fluid.

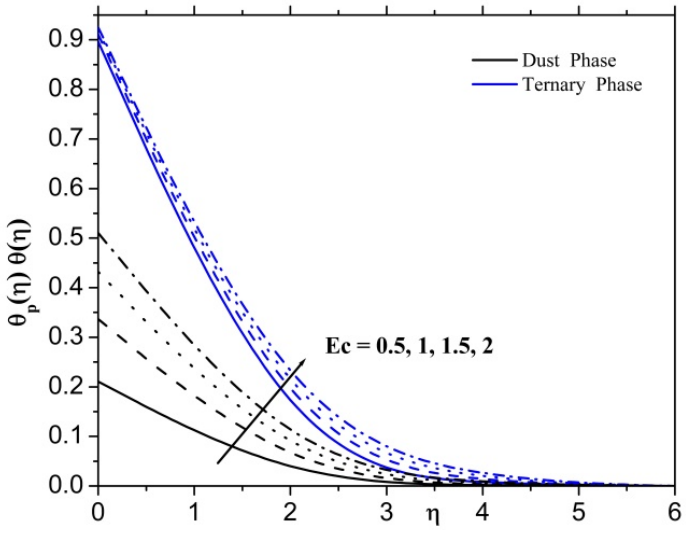

Figure 8. The $\theta(\eta)$ and $\theta_p(\eta)$ illustration against *Ec*.

In Figure 9, we see how varying the Γ parameter affects the thermal distribution for both $\theta(\eta)$ and $\theta_p(\eta)$ cases. It is inferred that when the Γ parameter increases, the fluid temperature decreases. An increase in the Γ parameter decreases the temperature field as it decelerates the relaxation of heat flow.

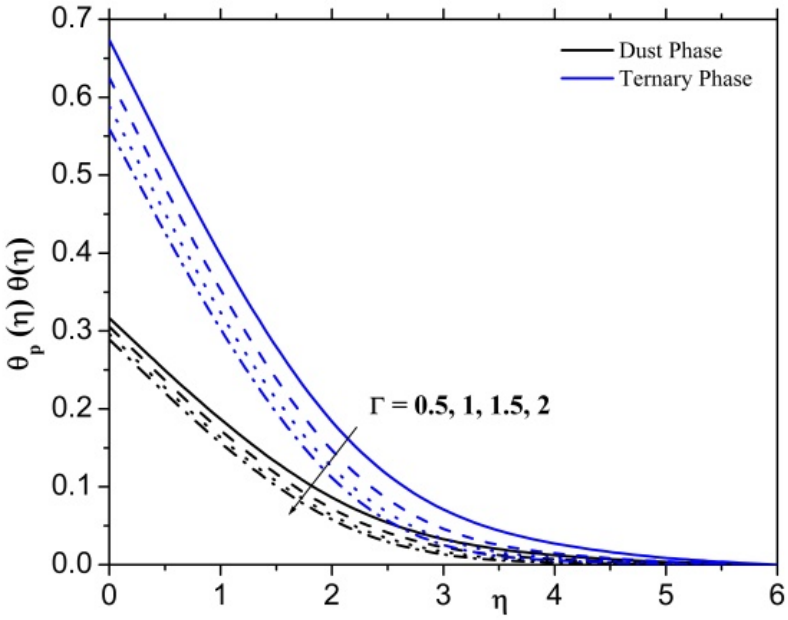

Figure 9. The $\theta(\eta)$ and $\theta_p(\eta)$ illustration against Γ.

The thermal field for the $\theta(\eta)$ and $\theta_p(\eta)$ instances is shown to be affected by the ϕ_1, ϕ_2, and ϕ_3 parameters in Figures 10–12. The fact that the nanoparticle is so tiny may be deduced from the amount of heat that it generates when it releases the accumulated energy. It is possible that in both cases ($\theta(\eta)$ and $\theta_p(\eta)$), extra energy will be needed for the mixing of additional nanoparticles. In turn, this will cause an increment in the temperature and the thickness of the associated layer.

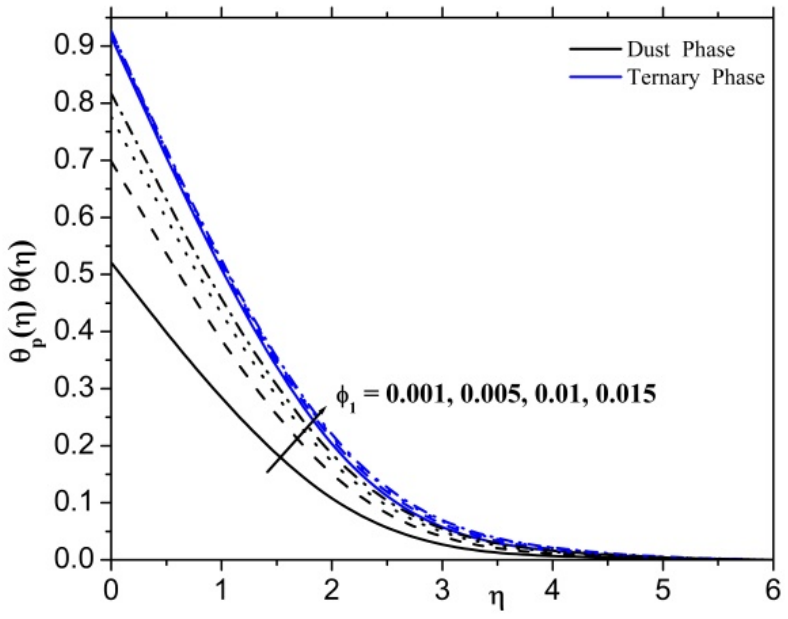

Figure 10. The $\theta(\eta)$ and $\theta_p(\eta)$ illustration against ϕ_1.

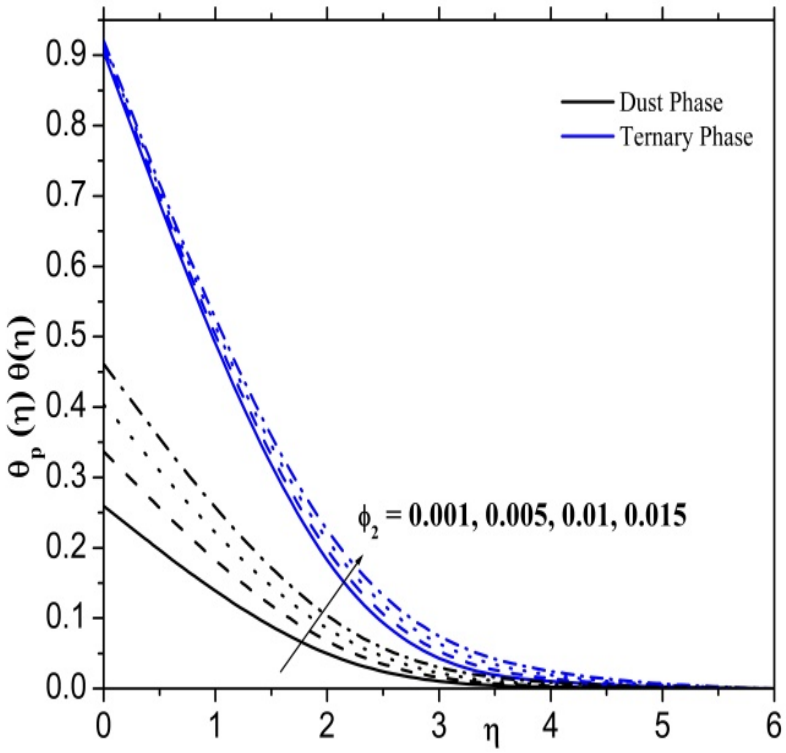

Figure 11. The $\theta(\eta)$ and $\theta_p(\eta)$ illustration against ϕ_2.

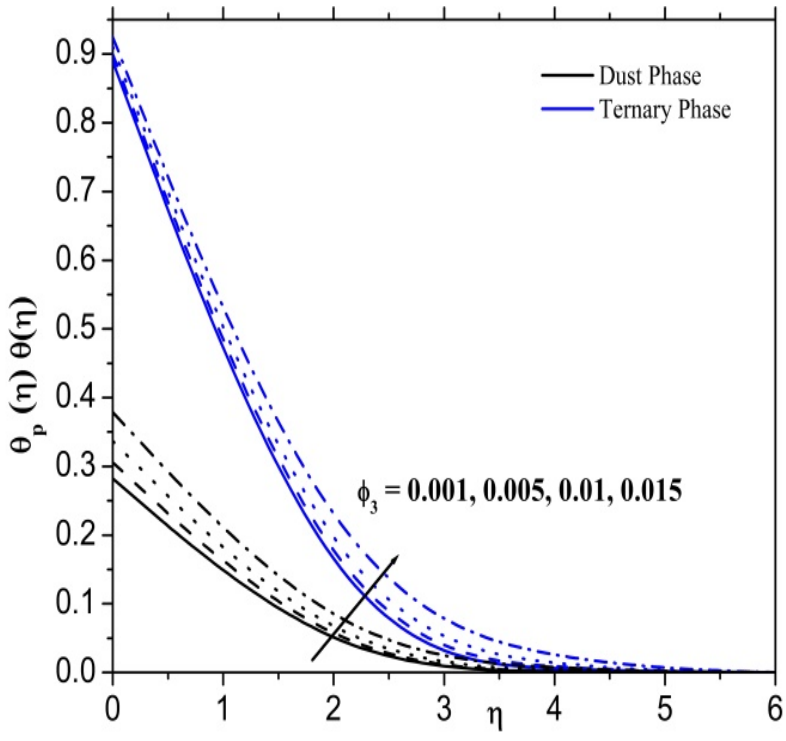

Figure 12. The $\theta(\eta)$ and $\theta_p(\eta)$ illustration against ϕ_3.

Figure 13 shows the effect of the Bi parameter on thermal field for both $\theta(\eta)$ and $\theta_p(\eta)$ instances. It is noted that the thermal field for both $\theta(\eta)$ and $\theta_p(\eta)$ instances increases with an increase in the Bi parameter. Furthermore, the interrelated thickness of the thermal layer also enhances by rising the values of the Bi parameter.

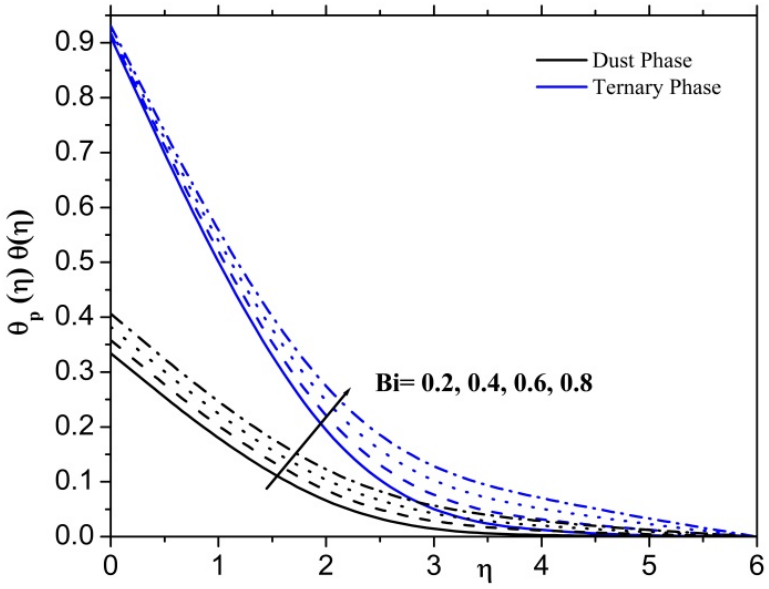

Figure 13. The $\theta(\eta)$ and $\theta_p(\eta)$ illustration against Bi.

In Tables 3 and 4, the impact of various substantial factors over skin friction and the Nusselt number for the fluid flow system has been portrayed in numerical manners. The fluid motion decreases with expansion in magnetic effects and slip factor. The friction factor decreases with augmenting values of the nanoparticle volume friction parameter (ϕ_1, ϕ_2, and ϕ_3), as shown in Table 3. The Nusselt number is maximized for higher values of the nanoparticle volume friction parameter (ϕ_1, ϕ_2, and ϕ_3), as shown in Table 4. An increment of the values of the Eckert number, Prandtl number, and Biot number enhances the Nusselt number. Additionally, the Nusselt number rises with the rising values of thermal relaxation. One can conclude that the Nusselt number is enhanced for higher values of radiation and temperature parameters.

5. Conclusions

By using a CC heat flux model, we investigated the movement of a dusty ternary nanofluid over a stretching sheet. The shown partial differential equations are converted to ordinary differential equations and numerically solved via the BVP4c technique. Graphs depict the concentration, the velocity, and the temperature. Overall, we are able to draw the following conclusions:

- The magnetic field depends essentially on Lorentz force, which is predominant for a larger magnetic field. Due to this, the velocity profiles decrease by further increasing the values of the magnetic parameter.
- The velocity profiles are decreasing by increasing the values of the slip parameter. However, once the slip velocity parameter is increased, the slide speed will also be decreased accordingly.
- The Eckert number is defined as the ratio between kinetic energy and the specific enthalpy difference between the wall and the fluid. Thus, increasing the Eckert number causes an increment in the temperature profile for both dusty and ternary phases.
- The thermal radiation role is to boost heat transfer by enlarging the thermal radiation and thermal boundary layers for both dusty and ternary phases.
- The tiny nanoparticle effect may be deduced from the amount of heat generated by the accumulated energy. Due to this, temperature profiles are enhanced by increasing values of the nanoparticle volume friction parameter.
- An increment in the value of thermal relaxation generates a decrement in the temperature distribution.

- Temperature profiles increase by increasing the values of the temperature ratio parameter.
- The performance of the dusty phase heat transfer has significantly enhanced compared to the performance of the ternary nanofluid phase.

Funding: This work was supported by the Deanship of Scientific Research, Vice Presidency for Graduate Studies and Scientific Research, King Faisal University, Saudi Arabia (Grant No. 2256).

Data Availability Statement: The data that support the findings of this study are available from the corresponding author upon reasonable request.

Acknowledgments: This work was supported by the Deanship of Scientific Research, Vice Presidency for Graduate Studies and Scientific Research, King Faisal University, Saudi Arabia (Grant No. 2256).

Conflicts of Interest: The authors declare no conflict of interest.

Nomenclature

B_0^2	Magnetic field
c_{pf}	Specific heat of fluid particle
c_{mf}	Specific heat of dust particle
C_f	Friction factor
Ec	Eckert number
K	Stokes drag coefficient
k_{thnf}	Thermal conductivity of the nano fluid
k_f	Thermal conductivity of the fluid
k^*	Mean absorption coefficient
l	Mass concentration of particles
m	Mass concentration of dust particles
Q	Magnetic parameter
N	Number density of dust particle
Nu	Nusselt number
Pr	Prandtl number
q_r	Radiative heat flux
R	Radiation parameter
u, u_p	Velocity along x axis $\left(m.s^{-1}\right)$
v, v_p	Velocity along y axis $\left(m.s^{-1}\right)$
Bi	Biot number
δ	Slip parameter
T_∞	Ambient fluid temperature
T_w	Wall temperature
T, T_p	Temperature of fluid and dust particle
Greek letters	
α	Ratio of specific heat
β_v	Fluid particle interaction parameter for velocity
β_t	Fluid particle interaction parameter for temperature
γ	Thermal relaxation parameter
τ_t	Relaxation time of dust particle for temperature
τ_v	Relaxation time of dust particle for velocity
λ_1	Relaxation time for heat flux
σ	Electrical conductivity
$\phi_1,\ \phi_2, \phi_3$	Volume fraction of nano particle
σ^*	Stefan Boltzmann constant
$\left(\rho c_p\right)$	Heat capacity of the fluid
$\left(\rho C_p\right)_{thnf}$	Heat capacity of the nanofluid
k_{thnf}	Thermal conductivity of ternary hybrid fluid
k_f	Thermal conductivity of fluid

References

1. Choi, U.; Eastman, J. Enhancing thermal conductivity of fluids with nanoparticles. In Proceedings of the 1995 International Mechanical Engineering Congress and Exhibition, San Francisco, CA, USA, 12–17 November 1995.
2. Buongiorno, J. Convective transport in nano fluids. *J. Heat Transf.* **2006**, *128*, 240–250. [CrossRef]
3. Reddy, M.; Rani, M.; Kumar, K.; Prasannakumar, B.; Lokesh, H. Hybrid dusty fluid flow through a Cattaneo–Christov heat flux model. *Phys. A Stat. Mech. Its Appl.* **2020**, *551*, 123975. [CrossRef]
4. Waqas, H.; Farooq, U.; Liu, D.; Abid, M.; Imran, M.; Muhammad, T. Heat transfer analysis of hybrid nanofluid flow with thermal radiation through a stretching sheet: A comparative study. *Int. Commun. Heat Mass Transf.* **2022**, *138*, 106303. [CrossRef]
5. Gürdal, M.; Pazarlıoğlu, H.K.; Tekir, M.; Arslan, K.; Gedik, E. Numerical investigation on turbulent flow and heat transfer characteristics of ferro-nanofluid flowing in dimpled tube under magnetic field effect. *Appl. Therm. Eng.* **2021**, *200*, 117655. [CrossRef]
6. Ashrafi, H.; Pourmahmoud, N.; Mirzaee, I.; Ahmadi, N. Performance improvement of proton-exchange membrane fuel cells through different gas injection channel geometries. *Int. J. Energy Res.* **2022**, *46*, 8781–8792.
7. Hussain, I.; Prakash, D.; Abdalla, B.; Muthtamilselvan, M. Analysis of Arrhenius activation energy and chemical reaction in nanofluid flow and heat transfer over a thin moving needle. *Curr. Nanosci.* **2023**, *19*, 39–48.
8. Sadiq, M.N.; Sajid, M.; Abbas, T.; Mahmood, K.; Bashir, S.; Mahmood, W. Numerical Simulation for flow and heat transfer of a nanofluid over lubricated stretchable surface. *J. Nanofluids* **2023**, *12*, 506–513. [CrossRef]
9. Prakasha, D.; Sudharani, M.; Kumar, K.G.; Chamkha, A.J. Comparative study of hybrid (graphene/magnesium oxide) and ternary hybrid (graphene/zirconium oxide/magnesium oxide) nanomaterials over a moving plate. *Int. Commun. Heat Mass Transf.* **2023**, *140*, 106557. [CrossRef]
10. Tiwari, R.K.; Das, M.K. Heat transfer augmentation in a two-sided liddriven differentially heated square cavity utilizing Nano fluids. *Int. J. Heat Mass Transf.* **2007**, *52*, 2002–2018.
11. Khilili, S.; Dinarvand, S.; Hosseini, R.; Saber, M.; Pop, I. Magnetohydrodynamic stagnation-point flow towards stretching/shrinking permeable plate in porous medium filled with a nano fluid. *J. Process Mech. Eng.* **2014**, *228*, 309–319.
12. Bakar, F.N.A.; Soid, S.K. MHD Stagnation-Point Flow and Heat Transfer Over an Exponentially Stretching/Shrinking Vertical Sheet in a Micropolar Fluid with a Buoyancy Effect. *J. Adv. Res. Numer. Heat Transf.* **2022**, *8*, 50–55.
13. Ali, A.; Marwat, D.N.K.; Ali, A. Analysis of flow and heat transfer over stretching/shrinking and porous surfaces. *J. Plast. Film. Sheeting* **2022**, *38*, 21–45. [CrossRef]
14. Azam, M.; Abbas, N.; Kumar, K.G.; Wali, S. Transient bioconvection and activation energy impacts on Casson nanofluid with gyrotactic microorganisms and nonlinear radiation. *Waves Random Complex Media* **2022**, 1–20. [CrossRef]
15. Reddy, M.G.; Krishnamurthy, M.R.; Praveena, M.M.; Naik, L.S.; Prakasha, D.G.; Kumar, K.G. Unsteady absorption flow and dissipation heat transfer over a non-Newtonian fluid. *Waves Random Complex Media* **2022**, 1–15. [CrossRef]
16. Reddy, M.G.; Sudharani, M.V.V.N.L.; Praveena, M.M.; Kumar, K.G. Effect of thermal conductivity on Blasius–Rayleigh–Stokes flow and heat transfer over a moving plate by considering magnetic dipole moment. *Eur. Phys. J. Plus* **2022**, *137*, 1–13.
17. Gil, P. Flow and heat transfer characteristics of single and multiple synthetic jets impingement cooling. *Int. J. Heat Mass Transf.* **2023**, *201*, 123590. [CrossRef]
18. Şahin, Y.S.; Toprak, B.I.; Solmaz, I.; Bayer, O. Investigation of flow and heat transfer behavior of integrated pin fin-aluminum foam heat sink. *Appl. Therm. Eng.* **2023**, *219*, 119504. [CrossRef]
19. Bejawada, S.G.; Nandeppanavar, M.M. Effect of thermal radiation on magnetohydrodynamics heat transfer micropolar fluid flow over a vertical moving porous plate. *Exp. Comput. Multiph. Flow* **2023**, *5*, 149–158. [CrossRef]
20. Gaur, P.K.; Jha, A.K. Heat Transfer for MHD Flow in an Inclined Channel with Heat Generation/Absorption. In *Advances in Mathematical Modelling, Applied Analysis and Computation*; Springer: Singapore, 2023; pp. 273–280.
21. Aljaloud, A.S.M. Hybrid nanofluid mixed convection in a cavity under the impact of the magnetic field by lattice Boltzmann method: Effects of barrier temperature on heat transfer and entropy. *Eng. Anal. Bound. Elem.* **2023**, *147*, 276–291. [CrossRef]
22. Yang, D.; Chen, L.; Feng, Y.; Chen, H. Comparisons of Supercritical Loop Flow and Heat Transfer Behavior Under Uniform and Nonuniform High-Flux Heat Inputs. *Nucl. Sci. Eng.* **2023**, *197*, 74–91. [CrossRef]
23. Fourier, J. *Théorie Analytique de Chaleur. chez Firmin Didot. Pere Et Fils*; Editions Jacques Gabay: Paris, France, 1822.
24. Cattaneo, C. Sulla conduzione del calore. *Atti Sem. Mat. Fis. Univ. Modena* **1948**, *3*, 83–101.
25. Christov, C.I. On frame indifferent formulation of the Maxwell-Cattaneo model of finite-speed heat conduction. *Mech. Res. Commun.* **2009**, *36*, 481–486. [CrossRef]
26. Reddy, M.; Vijayakumari, P.; Kumar, K.; Shehzad, S. Zero-mass flux and Cattaneo–Christov heat flux through a Prandtl non-Newtonian nanofluid in Darcy–Forchheimer porous space. *Heat Transf.* **2021**, *50*, 220–233. [CrossRef]
27. Machireddy, G.R.; Praveena, M.; Rudraswamy, N.G.; Kumar, G.K. Impact of Cattaneo–Christov heat flux on hydromagnetic flow of non-Newtonian fluids filled with Darcy–Forchheimer porous medium. *Waves Random Complex Media* **2021**, 1–18. [CrossRef]
28. Khan, S.A.; Hayat, T.; Alsaedi, A. Cattaneo Christov (CC) heat and mass fluxes in Stagnation point flow of Jeffrey nanoliquids by a stretched surface. *Chin. J. Phys.* **2022**, *76*, 205–216. [CrossRef]
29. Tausif, S.M.; Das, K.; Kundu, P.K. Modified Homogeneous and Heterogeneous Chemical Reaction and Flow Performance of Maxwell Nanofluid with Cattaneo–Christov Heat Flux Law. *J. Eng. Thermophys.* **2022**, *31*, 64–77. [CrossRef]

30. Hayat, T.; Fatima, A.; Muhammad, K.; Alsaedi, A. Heat transfer and entropy analysis in squeezing flow of hybrid nanofluid (Au-CuO/NaAlg) with DF (Darcy-Forchheimer) and CC (Cattaneo-Christov) heat flux. *Mater. Sci. Eng. B* **2023**, *288*, 116150. [CrossRef]
31. Ullah, H.; Ullah, K.; Raja, M.A.Z.; Shoaib, M.; Nisar, K.S.; Islam, S.; Weera, W.; Al-Harbi, N. Numerical treatment of squeezed MHD Jeffrey fluid flow with Cattaneo Chrisstov heat flux in a rotating frame using Levnberg-Marquard method. *Alex. Eng. J.* **2023**, *66*, 1031–1050. [CrossRef]
32. Shahzad, A.; Imran, M.; Tahir, M.; Khan, S.; Akgül; Abdullaev, S.; Yahia, I.S. Brownian motion and thermophoretic diffusion impact on Darcy-Forchheimer flow of bioconvective micropolar nanofluid between double disks with Cattaneo-Christov heat flux. *Alex. Eng. J.* **2023**, *62*, 1–15. [CrossRef]
33. Muhammad, K.; Hayat, T.; Alsaedi, A.; Momani, S. Mixed convective slip flow of hybrid nanofluid (MWCNTs + Cu + Water), nanofluid (MWCNTs + Water) and base fluid (Water): A comparative investigation. *J. Therm. Anal. Calorim.* **2021**, *143*, 1523–1536. [CrossRef]
34. Ghadikolaei, S.S.; Hosseinzadeh, K.; Hatami, M.; Ganji, D.D. MHD boundary layer analysis for micropolar dusty fluid containing Hybrid nanoparticles (Cu'Al2O3) over a porous medium. *J. Mol. Liq.* **2018**, *268*, 813–823. [CrossRef]
35. Hosseinzadeh, K.; Alizadeh, M.; Ganji, D.D. Hydrothermal analysis on MHD squeezing nanofluid flow in parallel plates by analytical method. *Int. J. Mech. Mater. Eng.* **2018**, *13*, 4. [CrossRef]